The Use of Large-Eddy Simulations in Lagrangian Particle Dispersion Models

JEFFREY C. WEIL

CIRES, University of Colorado, Boulder, Colorado

PETER P. SULLIVAN AND CHIN-HOH MOENG

National Center for Atmospheric Research, Boulder, Colorado*

(Manuscript received 5 January 2004, in final form 25 May 2004)

ABSTRACT

A Lagrangian dispersion model driven by velocity fields from large-eddy simulations (LESs) is presented for passive particle dispersion in the planetary boundary layer (PBL). In this combined LES–Lagrangian stochastic model (LSM), the total velocity is divided into resolved or filtered and unresolved or subfilter-scale (SFS) velocities. The random SFS velocity is modeled using an adaptation of Thomson's LSM in which the ensemble-mean velocity and velocity variances are replaced by the resolved velocity and SFS variances, respectively. The random SFS velocity forcing has an amplitude determined by the SFS fraction of the total turbulent kinetic energy (TKE); the fraction is about 0.15 in the bulk of the simulated convective boundary layer (CBL) used here and reaches values as large as 0.31 and 0.37 in the surface layer and entrainment layer, respectively.

For the proposed LES–LSM, the modeled crosswind-integrated concentration (CWIC) fields are in good agreement with the 1) surface-layer similarity (SLS) theory for a surface source in the CBL and 2) convection tank measurements of the CWIC for an elevated release in the CBL surface layer. The second comparison includes the modeled evolution of the vertical profile shape with downstream distance, which shows the attainment of an elevated CWIC maximum and a vertically well-mixed CWIC far downstream, in agreement with the tank data. For the proposed model, the agreement with the tank data and SLS theory is better than that obtained with an earlier model in which the SFS fraction of the TKE is assumed to be 1, and significantly better than a model that neglects the SFS velocities altogether.

1. Introduction

Turbulent dispersion of scalars is probably best understood in a Lagrangian framework as first suggested by Taylor's (1921) statistical theory of dispersion in homogeneous turbulence. However, for dispersion in many flows such as the planetary boundary layer (PBL), one must deal with the complexities due to inhomogeneous, nonstationary, and non-Gaussian turbulence. These complications can be addressed with Lagrangian stochastic models (LSMs), which describe the trajectories of ''passive'' particles in a turbulent flow given the random velocity field (e.g., Thomson 1987; Wilson and Sawford 1996); for complex turbulence fields, the particle velocity must be computed numerically. By simulating thousands of particle trajectories, one can find the ensemble-mean concentration, which is proportional to the particle number density, that is, the probability density function (PDF) of particle position.

Thomson (1987) gave a rigorous basis for constructing an LSM as outlined in section 3. In his approach, the stochastic differential equation for the Lagrangian velocity requires an assumed form of the Eulerian velocity PDF and the velocity moments (e.g., variances) defining it. In applications, the moments are provided by parameterized profiles fitted to laboratory and field data or numerical simulations. For inhomogeneous turbulence, the formulation leads to a unique solution for dispersion in one dimension, which is typically the vertical direction in PBL applications. However, for three-dimensional dispersion, there is no generally unique solution, but there are particular solutions that are useful (Wilson and Sawford 1996).

Another method for driving the particles in a Lagrangian model is with the time-dependent velocity fields from a large-eddy simulation (LES). This approach was pioneered by Lamb (1978) who numerically computed dispersion due to an elevated source in the convective boundary layer (CBL). He adopted Deardorff's (1974) LES results and decomposed the Lagrangian velocity $\mathbf{u}_L$ of a particle into resolved and sub-

* The National Center for Atmospheric Research is sponsored by the National Science Foundation.

Corresponding author address: Dr. Jeffrey C. Weil, NCAR/MMM, P.O. Box 3000, Boulder, CO 80307-3000.
E-mail: weil@ucar.edu

filter-scale (SFS) components (see section 2) consistent with the LES:

$$\mathbf{u}_L(\mathbf{x}_{os}, t) = \mathbf{u}_r[\mathbf{x}_p(\mathbf{x}_{os}, t), t] + \mathbf{u}_s[\mathbf{x}_p(\mathbf{x}_{os}, t), t], \quad (1)$$

where $\mathbf{x}_{os}$ is the source or initial particle position, t is time, $\mathbf{u}_r$ is the LES resolved velocity at each grid point and time step, $\mathbf{x}_p(\mathbf{x}_{os}, t)$ is the particle position at t, and $\mathbf{u}_s$ is a random SFS velocity (bold-faced symbol denotes a vector). The $\mathbf{u}_s$ was found from a Monte Carlo scheme using the SFS energy. Lamb's results for the mean concentration field and particle displacement statistics agreed well with Willis and Deardorff's (1978) convection tank data, thus providing much support for the combined LES–LSM approach.

In later work, Mason (1992) adopted a similar approach and investigated dispersion over a range of wind shear in the PBL. However, instead of using Eq. (1), he superposed the displacements due to the resolved and SFS motions, where the SFS contribution was found from a random displacement model using a parameterized eddy diffusivity. Mason found a fairly systematic variation of the dispersion with surface shear. However, he noted that it would have been better to include the SFS turbulent kinetic energy (TKE) directly in the model since, in the high wind cases, such energy was a large fraction of the resolved TKE in the PBL surface layer. More recently, Gopalakrishnan and Avissar (2000) used LES velocity fields to study dispersion in the CBL in the presence of surface heterogeneities. However, they neglected the SFS velocities altogether because they felt there was no adequate scheme for treating them.

A Lagrangian model based on the LES–LSM approach has the main advantage of dealing with dispersion over a wide range of PBL types and forcings (mean wind, surface heat flux, etc.), as well as an arbitrary source height. The resolved velocity field is unique and any issue of nonuniqueness is deferred to the SFS component, where it should be less serious. However, one must formulate an acceptable if only simple treatment of the random SFS velocity.

This paper addresses the use of LES fields in Lagrangian dispersion models with focus on the SFS treatment. Section 2 gives a brief overview of LES, and section 3 presents an outline of Thomson's (1987) LSM and our adaptation of it to include LES fields. In section 4, we show example results from this combined LES–LSM approach for surface-layer sources in the CBL and compare them with laboratory data and surface-layer similarity theory (van Ulden 1978; Horst 1979).

2. Large-eddy simulations

Large-eddy simulation of the PBL is well established (e.g., Mason 1994; Moeng and Wyngaard 1988), and thus we give only a brief overview of the method as well as some details of the LES model used here (Moeng and Sullivan 1994). Most LESs of the PBL adopt the incompressible Boussinesq form of the Navier–Stokes equations and consider a horizontally homogeneous boundary layer. The flow variables (three wind components, pressure, temperature, etc.) are spatially filtered to define resolved components, which have length scales larger than the filter width, and SFS components, alternatively called subgrid-scale components. The filter width is of the order of the numerical grid dimension and lies in the inertial subrange of the turbulence spectrum. The filtered Navier–Stokes equations are solved to determine the resolved variables, while the SFS quantities—TKE, momentum fluxes, and heat fluxes—are parameterized. The filtered equations depend on the SFS variables, but the dependence is weak provided that the SFS TKE is only a small fraction of the total. The SFS TKE fraction is generally small (~15% to 20%) in the bulk of the PBL for a typical LES grid resolution, but this is not the case near the surface and in the entrainment zone (see section 3).

In the Moeng and Sullivan (1994) model, the SFS TKE is found from a prognostic equation, while the SFS fluxes are obtained from a first-order closure or flux–gradient model. For example, the SFS momentum flux or stress tensor τ_{ij} is given by

$$\tau_{ij} = -\nu_t\left(\frac{\partial u_{ri}}{\partial x_j} + \frac{\partial u_{rj}}{\partial x_i}\right), \quad (2)$$

where $i, j = 1, 2, 3$ corresponding to the x, y, z directions, respectively, and ν_t is the turbulent eddy viscosity. The ν_t is parameterized by

$$\nu_t = c_k \ell e_s^{1/2}, \quad (3)$$

where c_k is a constant (=0.1), ℓ is a mixing length, and e_s is the SFS TKE. The SFS heat flux is given by a form similar to Eq. (2), and the turbulence dissipation rate ϵ is parameterized by

$$\epsilon = c_\epsilon \frac{e_s^{3/2}}{\ell}, \quad (4)$$

where c_ϵ is a constant (=0.93) in neutral and unstable stratification.

For neutral or unstable conditions, $\ell = \Delta$, the filter width, whereas for stable stratification, $\ell = \min(\Delta, \ell_{st})$, where ℓ_{st} is a length scale (Deardorff 1980) that accounts for the reduced mixing imposed by the stratification:

$$\ell_{st} = \frac{0.76 e_s^{1/2}}{[(g/\Theta_o)(\partial\theta_r/\partial z)]^{1/2}}, \quad (5)$$

where g is the gravitational acceleration, θ_r is the resolved potential temperature, and Θ_o is a reference potential temperature. The filter width used above is $\Delta = [(3/2)^2 \Delta x \Delta y \Delta z]^{1/3}$, where Δx, Δy, and Δz are the mesh spacings in the three coordinate directions x, y, z, and the factor $(3/2)^2$ accounts for the explicit filtering of the upper one-third of the wavenumbers, that is, dealiasing. Here, x is in the mean geostrophic wind direction, y is perpendicular to x and lies in the horizontal plane, and z is the height above the surface.

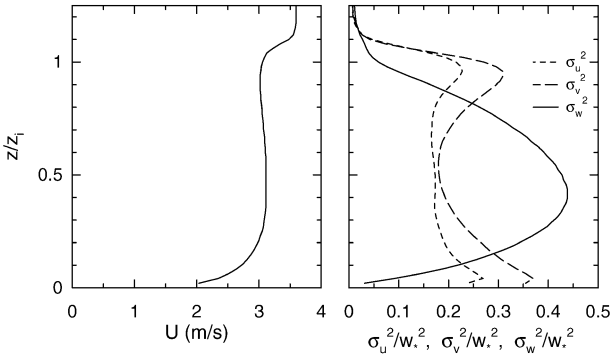

FIG. 1. (a) Mean horizontal wind speed and (b) resolved velocity variances normalized by w_*^2 both as functions of dimensionless height in the CBL; $-z_i/L = 106$.

For the particle dispersion calculations discussed later, the LESs were made for a CBL using a 5 km × 5 km × 2 km domain with 96^3 grid points; this resulted in $\Delta x = \Delta y \simeq 52$ m, $\Delta z \simeq 21$ m, and $\Delta \simeq 50$ m. The surface heat flux was $\overline{w\theta}_o = 0.24$ m s^{-1} K, and the average CBL depth z_i was 1000 m over the simulation period of $10z_i/w_*$. Based on these values, the convective velocity scale $w_* = (g\overline{w\theta}_o z_i/\Theta_o)^{1/3}$ was 2 m s^{-1}. Other variables in the LES were the surface roughness length z_0 (0.16 m), the average friction velocity u_* (0.31 m s^{-1}), the vertically averaged wind speed U over the CBL (3 m s^{-1}), and the Monin–Obukhov (M–O) length L (−9.4 m).

The stability index $-z_i/L$ characterizing the relative strengths of convective and shear-generated turbulence (Deardorff 1972) was 106 and would classify the CBL as highly convective. In this case, the mean wind profile is close to a well-mixed state over most of the CBL (Fig. 1a), and the velocity variances exhibit profiles typical of strong or free convection (Fig. 1b), for example, see Deardorff and Willis (1985).

3. Lagrangian dispersion models

In Lagrangian dispersion models, passive ''particles'' released into a turbulent flow are assumed to behave as fluid elements and to travel with the local fluid velocity with molecular diffusion ignored. The mean concentration C is found from (Lamb 1978)

$$C(\mathbf{x}, t) = \int_{-\infty}^{t} Q(t') p_1(\mathbf{x}, t; \mathbf{x}_{os}, t')\, dt', \qquad (6)$$

where Q is the source strength, which is time dependent in general; however, in the following, we only consider a steady or constant Q. In (6), $p_1(\mathbf{x}, t; \mathbf{x}_{os}, t')$ is the position PDF for particles released at the source position $\mathbf{x}_{os}$ at time t' being found at $\mathbf{x}$ at time t; p_1 is computed from the numerically calculated particle trajectories. The particle position $\mathbf{x}_p$ is found by integrating

$$\frac{d\mathbf{x}_p}{dt} = \mathbf{u}_L(\mathbf{x}_{os}, t). \qquad (7)$$

As noted earlier, there are two ways of finding the Lagrangian velocities for particle tracking: 1) from a purely stochastic model that requires an assumed Eulerian velocity PDF (Thomson 1987) and 2) from the time-dependent velocity fields from an LES. In the following, we give a brief review of Thomson's approach and then show how it is adapted to include LES fields, and in particular, to obtain a stochastic model for the SFS velocity in Eq. (1).

a. Lagrangian stochastic model (Thomson 1987)

In the case of nonstationary and inhomogeneous turbulence, Thomson's (1987) form for the ith component of the Lagrangian velocity u_{Li} is the stochastic differential equation

$$du_{Li} = a_i(\mathbf{x}_p, \mathbf{u}_L, t)dt + (C_0\overline{\epsilon})^{1/2} d\xi_i, \qquad (8)$$

where a_i is a ''drift velocity'' or deterministic velocity forcing function, $(C_0\overline{\epsilon})^{1/2} d\xi_i$ is the random velocity forcing, and the overbar denotes an ensemble mean. Here, $d\xi_i$ is a component of a Gaussian white noise, which is uncorrelated with components in other directions and uncorrelated in time, and C_0 is an assumed universal constant (=4 ± 2; Thomson 1987). Thomson chose the form of the random forcing to be consistent with the Lagrangian structure function in the inertial subrange (Monin and Yaglom 1975): $\overline{du_{Li}du_{Lj}} = \delta_{ij}C_0\overline{\epsilon}dt$, where δ_{ij} is the Kronecker delta.

For a Gaussian random forcing, the a_i and the coefficient of the random forcing $(C_0\overline{\epsilon})^{1/2}$ must satisfy the Fokker–Planck equation, which governs the evolution of the joint PDF $p(\mathbf{x}_p, \mathbf{u}_L, t)$ of $\mathbf{x}_p$ and $\mathbf{u}_L$ in phase space (see Thomson 1987; Gardiner 1990). Thomson found a_i by imposing the ''well mixed'' condition, which assumes that if particles are initially well mixed in some region, they remain so. For a well-mixed distribution of particles, the joint PDF $p(\mathbf{x}_p, \mathbf{u}_L, t) = p_E(\mathbf{x}, \mathbf{u}, t)$, the Eulerian velocity PDF, since there is no single source or labeling point to distinguish the Lagrangian statistics from the Eulerian statistics. In this case, Thomson argued that the a_i in Eq. (8) could be obtained from the Fokker–Planck equation using p_E, which is known or assumed. For three-dimensional dispersion, there is a unique solution for a_i in only a few special cases, for example, homogeneous isotropic turbulence (see Wilson and Sawford 1996).

For three-dimensional Gaussian turbulence, the Eulerian velocity PDF is given by

$$p_E = \frac{1}{(2\pi)^{3/2}(\det\overline{\tau}_{ij})^{1/2}} \times \exp\left[-\frac{1}{2}(u_i - U_{Ei})\overline{\lambda}_{ij}(u_j - U_{Ej})\right], \qquad (9)$$

where $\overline{\tau}_{ij}$ is the three-dimensional ensemble-mean stress tensor, $\overline{\lambda}_{ij}$ is its inverse, and u_i and U_{Ei} are the ith components of the total and ensemble-mean Eulerian velocities, respectively (Thomson 1987). In the case of inhomogeneous Gaussian turbulence, Thomson found a_i to be

$$a_i = -\frac{C_0\overline{\epsilon}}{2}\overline{\lambda}_{ik}(u_k - U_{Ek}) + \frac{\phi_i}{p_E}, \tag{10}$$

where ϕ_i/p_E is

$$\frac{\phi_i}{p_E} = \frac{1}{2}\frac{\partial\overline{\tau}_{il}}{\partial x_l} + \frac{\partial U_{Ei}}{\partial t} + U_{El}\frac{\partial U_{Ei}}{\partial x_l} + \left[\frac{1}{2}\overline{\lambda}_{lj}\left(\frac{\partial\overline{\tau}_{il}}{\partial t} + U_{Em}\frac{\partial\overline{\tau}_{il}}{\partial x_m}\right) + \frac{\partial U_{Ei}}{\partial x_j}\right](u_j - U_{Ej}) + \frac{1}{2}\overline{\lambda}_{lj}\frac{\partial\overline{\tau}_{il}}{\partial x_k}(u_j - U_{Ej})(u_k - U_{Ek}). \tag{11}$$

A derivation of the above form can be found in Rodean (1996). This form is used in the next section to obtain a stochastic model for $\mathbf{u}_s$.

b. Lagrangian model with LES fields coupled with an LSM

In using LES fields to model particle dispersion, we substitute Eq. (1) into Eq. (7) and integrate the latter to obtain the particle postion. However, we first must prescribe the SFS velocity $\mathbf{u}_s$, which we do using an adaptation of Thomson's model for the local or grid-volume level. We assume that 1) the ensemble-mean velocity (U_{Ei}) in Eqs. (9)–(11) can be replaced by the LES resolved velocity u_{ri}, which is an effective average over a grid volume, 2) the LSM describes the random SFS velocity about u_{ri}, 3) the SFS velocities are specified by a Gaussian PDF based on the SFS stress tensor τ_{ij} and its inverse λ_{ij}, and 4) the $\overline{\epsilon}$ can be replaced by the local value ϵ. The aim of the first assumption is to remove u_{ri} from the LSM treatment since it is provided by the LES and already included in Eq. (1). The assumption should be valid provided that the change (δu_{ri}) in u_{ri} during particle transport through a grid is small, $\delta u_{ri}/u_{ri} \ll 1$. This in turn should be satisfied if the resolved velocity advection time $t_{\rm ad} \ll T_{Er}$, the Eulerian time scale of u_{ri}. The $t_{\rm ad}$ can be estimated as $\sim\Delta/U$, and $T_{Er} \sim \ell_E/U$ (Pasquill and Smith 1983), where ℓ_E is the large-eddy length scale. In the midregion of the CBL, $\ell_E \sim z_i$ and $t_{\rm ad}/T_{Er} \sim (\Delta/U)/(z_i/U) = \Delta/z_i = 0.05$ for the grid adopted here (section 2). Thus, the assumption is easily satisfied in the bulk of the CBL.

By the first assumption, we replace the U_{Ei} in Eqs. (10) and (11) by u_{ri} and note that the difference $u_i - u_{ri} = u_{si}$, the random SFS velocity; we also replace $\overline{\tau}_{ij}$ and $\overline{\lambda}_{ij}$ by their SFS counterparts τ_{ij} and λ_{ij}. With these substitutions and recalling that $du_{ri}/dt = \partial u_{ri}/\partial t + (u_{rk} + u_{sk})(\partial u_{ri}/\partial x_k)$ and similarly for $d\tau_{il}/dt$, we can rewrite Eq. (11) in the simple form

$$\frac{\phi_i}{p_E} = \frac{1}{2}\frac{\partial\tau_{il}}{\partial x_l} + \frac{du_{ri}}{dt} + \frac{1}{2}\lambda_{lj}\frac{d\tau_{il}}{dt}u_{sj}. \tag{12}$$

Equation (10) with $u_k - U_{Ek}$ replaced by u_{sk} and Eq. (12) can be substituted into Eq. (8) to obtain the following equation for the Lagrangian velocity increment

$$du_{Li} = -\frac{C_0\epsilon}{2}\lambda_{ik}u_{sk}dt + \left(\frac{1}{2}\frac{\partial\tau_{il}}{\partial x_l} + \frac{du_{ri}}{dt} + \frac{1}{2}\lambda_{lj}\frac{d\tau_{il}}{dt}u_{sj}\right)dt + (C_0\epsilon)^{1/2}d\xi_i. \tag{13}$$

By subtracting du_{ri} from both sides of Eq. (13), we find a stochastic differential equation governing u_{si}

$$du_{si} = -\frac{f_sC_0\epsilon}{2}\lambda_{ik}u_{sk}dt + \frac{1}{2}\left(\lambda_{lj}\frac{d\tau_{il}}{dt}u_{sj} + \frac{\partial\tau_{il}}{\partial x_l}\right)dt + (f_sC_0\epsilon)^{1/2}d\xi_i. \tag{14}$$

In Eq. (14), the random forcing term has been modified by introducing the coefficient f_s ($f_s \le 1$) to account for the SFS velocities that are being modeled, which are smaller than the u_{Li} in Eq. (13). A parameterization for f_s is discussed below.

Equation (14) can be simplified by assuming that the SFS turbulence is locally isotropic and Gaussian but weakly inhomogeneous. The local isotropy assumption is consistent with most LES models at least in mid-PBL regions where the turbulence is well resolved (e.g., Moeng and Wyngaard 1988). The assumption does not hold near the surface where wind shear effects are important (Sullivan et al. 2003). For isotropic turbulence, the stress tensor is diagonal with components given by $\sigma_s^2 = 2e_s/3$, and the inverse tensor also is diagonal with components σ_s^{-2}. Thus, the resulting equation for the SFS velocity is

$$du_{si} = -\frac{f_sC_0\epsilon}{2}\frac{u_{si}}{\sigma_s^2}dt + \frac{1}{2}\left(\frac{1}{\sigma_s^2}\frac{d\sigma_s^2}{dt}u_{si} + \frac{\partial\sigma_s^2}{\partial x_i}\right)dt + (f_sC_0\epsilon)^{1/2}d\xi_i. \tag{15}$$

A parameterization for f_s is developed by considering stationary homogeneous isotropic turbulence, which leads to a simple expression [Eq. (22) below]. In developing this expression, we focus only on the vertical velocity w and decompose it into resolved (r) and SFS (s) components: $w = w_r + w_s$. We assume that w, w_r, and w_s are characterized by their respective variances σ_w^2, σ_{rw}^2, σ_{sw}^2, and that $\sigma_w^2 = \sigma_{rw}^2 + \sigma_{sw}^2$, where we ignore the cross term $\overline{w_rw_s}$. In addition, we assume that Lagrangian velocities corresponding to each component (e.g., w_{Ls}) can be represented by a stochastic differential equation of the form

$$dw_{L\alpha} = -\frac{w_{L\alpha}dt}{T_{L\alpha}} + \left(\frac{2\sigma_{\alpha w}^2}{T_{L\alpha}}\right)^{1/2} d\xi, \qquad (16)$$

where $\alpha = r$, s or a blank; that is, no second subscript denotes the total velocity w_L. Here, the term $C_0\epsilon$ in the random forcing has been written in an equivalent form $C_0\epsilon = 2\sigma_w^2/T_L$ (see Sawford 1991; Rodean 1996) so that the appropriate variance and time scale of each component (e.g., r or s) is represented in (16); for example, $f_s C_0\epsilon = 2\sigma_{sw}^2/T_{Ls}$. In adopting Eq. (16), we are effectively assuming that the Lagrangian energy density spectra for the r and s components have the same shape (density $\propto -2$ power of the frequency; e.g., Tennekes and Lumley 1972) but a different total energy content or variance. This assumption is believed to be most applicable near the surface, where σ_{sw}^2 and σ_{rw}^2 are comparable and the SFS and resolved energy spectra are not widely separated; that is, where Δ is of the order of z or the characteristic eddy size. However, in general, the assumed spectral shape similarity differs from the results of LES filtering and requires further investigation. Nevertheless, we believe that the above parameterization is adequate to obtain an initial estimate of the SFS time scale.

Our goal is to determine the time scale (T_{Ls}) of the SFS component and thereby the magnitude of f_s. The main criterion to satisfy is that the Lagrangian autocorrelation function for the summed velocity $w_{Lr} + w_{Ls}$ be the same as that for the total velocity w_L. This ensures that the random velocity decorrelates in the same manner whether it is decomposed into r and s components or not.

We follow Durbin (1983) in obtaining the autocorrelation function R_L for the stochastic velocity $w_L(t)$ by first writing Eq. (16) for $dw_L(t + \tau)$, where τ is a time lag, multiply the equation by $w_L(t)$, and perform an ensemble average. Note that the ensemble average of $\overline{w_L(t)d\xi(t + \tau)} = 0$ due to the nonanticipating property of $w_L(t)$, which means that $w_L(t)$ is statistically independent of the random increment $d\xi(t + \tau)$ for $\tau \geq 0$ (Durbin 1983; Gardiner 1990). The result is

$$\frac{d\overline{w_L(t)w_L(t + \tau)}}{d\tau} = -\frac{\overline{w_L(t)w_L(t + \tau)}}{T_L}, \qquad (17)$$

which has the solution

$$R_L(\tau) = \frac{\overline{w_L(t)w_L(t + \tau)}}{\sigma_w^2} = \exp\left(-\frac{\tau}{T_L}\right), \qquad (18)$$

as shown by Durbin (1983); in Eq. (18), $\sigma_w^2 = \overline{w^2}$, the ensemble-mean variance.

In a similar way, the equations governing the autocorrelations of w_{Lr} and w_{Ls} can be found as

$$\frac{d\overline{w_{L\alpha}(t)w_{L\alpha}(t + \tau)}}{d\tau} = -\frac{\overline{w_{L\alpha}(t)w_{L\alpha}(t + \tau)}}{T_{L\alpha}}, \qquad (19)$$

with $\alpha = r$ or s. The autocorrelation functions for w_{Lr} and w_{Ls} are also of exponential form and depend on their respective time scales, T_{Lr} and T_{Ls}. Equations for the cross-correlation functions $\overline{w_{Lr}(t)w_{Ls}(t + \tau)}$ and $\overline{w_{Ls}(t)w_{Lr}(t + \tau)}$ can be obtained similarly. The equations for the auto- and cross-correlation functions can be added to obtain the autocorrelation for the summed velocity $w_{Lr} + w_{Ls}$ as

$$\begin{aligned}\frac{d}{d\tau}&[\overline{w_{Lr}(t)w_{Lr}(t + \tau)} + \overline{w_{Ls}(t)w_{Lr}(t + \tau)} \\ &+ \overline{w_{Lr}(t)w_{Ls}(t + \tau)} + \overline{w_{Ls}(t)w_{Ls}(t + \tau)}] \\ &= -\frac{\overline{w_{Lr}(t)w_{Lr}(t + \tau)}}{T_{Lr}} - \frac{\overline{w_{Ls}(t)w_{Lr}(t + \tau)}}{T_{Lr}} \\ &\quad - \frac{\overline{w_{Lr}(t)w_{Ls}(t + \tau)}}{T_{Ls}} - \frac{\overline{w_{Ls}(t)w_{Ls}(t + \tau)}}{T_{Ls}}. \qquad (20)\end{aligned}$$

Equation (20) has the same solution as Eq. (17) only if $T_{Ls} = T_{Lr} = T_L$. The equality $T_{Ls} = T_L$ means that the coefficient of the SFS random forcing in Eq. (16) should be $(2\sigma_{ws}^2/T_L)^{1/2}$. By dividing the random forcing coefficient of the SFS component $[(f_s C_0\epsilon)^{1/2} = (2\sigma_{sw}^2/T_L)^{1/2}]$ by the coefficient for the total velocity $[(C_0\epsilon)^{1/2} = (2\sigma_w^2/T_L)^{1/2}]$, we find $f_s = \sigma_{sw}^2/\sigma_w^2$ or

$$f_s = \frac{\sigma_{sw}^2}{\sigma_{rw}^2 + \sigma_{sw}^2}. \qquad (21)$$

The above form for f_s is adopted in Eq. (15) except that we replace σ_{sw}^2 by $\langle\sigma_s^2\rangle$ and σ_{rw}^2 by $\langle\sigma_{av}^2\rangle$ or

$$f_s = \frac{\langle\sigma_s^2\rangle}{\langle\sigma_{av}^2\rangle + \langle\sigma_s^2\rangle}, \qquad (22)$$

where $\sigma_{av}^2 = (\sigma_{ru}^2 + \sigma_{rv}^2 + \sigma_{rw}^2)/3$ and the angle brackes $\langle\ \rangle$ denote an average over the horizontal plane. The f_s can be viewed equivalently as the SFS fraction of the total TKE, $f_s = \langle e_s\rangle/(\langle e_r\rangle + \langle e_s\rangle)$, since $\sigma_{av}^2 = 2e_r/3$, where e_r is the resolved TKE. The fraction can range from 0, where the turbulence is entirely resolved (i.e., a zero SFS velocity), to 1, where the turbulence is completely parameterized by the LSM.

Figure 2a shows that the horizontally averaged SFS and resolved-scale TKE vary little with height over the

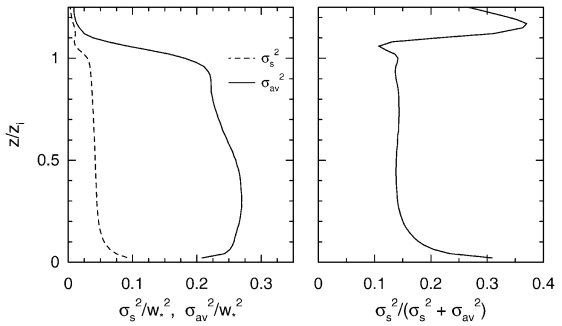

FIG. 2. (a) Horizontally averaged values of resolved and subfilter-scale velocity variances normalized by w_*^2 and (b) SFS fraction of total TKE both as functions of dimensionless height.

bulk of the simulated CBL, $0.1 \leq z/z_i \leq 1$, where the SFS TKE fraction (Fig. 2b) is ~0.15. The primary regions of variation are in the surface layer ($z/z_i < 0.1$) and the entrainment zone ($0.85z_i \lesssim z \lesssim 1.2z_i$) as shown by the SFS TKE fraction (Fig. 2b); the fraction attains values as large as 0.31 and 0.37 in the surface layer and entrainment zones, respectively. The fraction is expected to approach 1 at the surface since the resolved velocity components vanish there.

4. Application to a highly convective boundary layer

a. Modeling the crosswind-integrated concentration

We first describe the approach for obtaining the crosswind-integrated concentration (CWIC) field from the particle position PDF and then outline the method for computing the PDF. The CWIC C^y, due to a continuous point source, is

$$C^y(x, z, t) = \int_{-\infty}^{\infty} C(x, y, z, t)\, dy, \tag{23}$$

where C is the mean concentration, x is now alligned with the mean wind direction in the CBL, and y is normal to x in the horizontal plane. For horizontally homogeneous and stationary turbulence, we can write Eq. (6) in terms of the x, y, z, and time displacements as $C(\mathbf{x}, t) = Q \int_{-\infty}^{t} p_1(\mathbf{x} - \mathbf{x}_{os}, t - t')\, dt'$. By substituting this into Eq. (23), we obtain the C^y field as

$$C^y(x, z, t) = Q \int_{-\infty}^{t} p_1(x - x_{os}, z - z_{os}, t - t')\, dt'. \tag{24}$$

With a variable change from t' to $t_d = t - t'$, Eq. (24) can be written in the alternative form

$$C^y(x, z) = Q \int_{0}^{\infty} p_1(x - x_{os}, z - z_{os}, t_d)\, dt_d. \tag{25}$$

In practice, the upper integration limit is set sufficiently large, $t_d = t_f$, so that we accurately determine the integral at the largest sampling distance x_e of interest. We found that $t_f = 1.5x_e/U$ was large enough for convergence of the above integral and have used this t_f in the following.

The particle displacements necessary for computing p_1 and hence C^y were found by integrating Eq. (15) to find u_{si}, substituting u_{si} and u_{ri} (from the LES) into Eq. (1), and inserting the resultant $\mathbf{u}_L$ into Eq. (7) and integrating. The mean CWIC fields were obtained by superposing the position PDFs from 81 equally spaced sources at height z_{os} in a horizontal plane; the source spacing in the x and y directions was set at $\simeq 0.5z_i$ so that the particle velocities from adjacent sources would be approximately independent. At each source, 60 particles were released, each with a random initial SFS velocity. The releases were made at 15 equally spaced times over a 28-min period ($\simeq 3.4z_i/w_*$) and resulted in a total of 72 900 particles released.

The particle trajectory calculations were conducted with instantaneous velocity fields that were input sequentially from a large number (500) of LES files. The files were stored at 10-s or $0.02z_i/w_*$ time intervals and each contained a 96^3 array of $\mathbf{u}_r$, e_s, and potential temperature; the total time period covered was $10z_i/w_*$. In the trajectory computations, the local values of $\mathbf{u}_r$ and e_s were found from trilinear spatial interpolation within each LES grid and time interpolation between two successive LES files. The time step in the trajectory computations [Eq. (15)] was $\min(0.025T_L, 0.4\Delta t_d)$, where $\Delta t_d = 0.005z_i/w_*$ was the time step used in the particle sampling grid [Eq. (25)]. A reflection of particle height and the SFS vertical velocity w_s was assumed at the surface to satisfy the zero-flux condition there. For particles that rose above the instantaneous z_i, the w_s was reversed or reflected at the height (z_r) of the reversal in the resolved vertical velocity w_r if w_s and w_r were both positive; the z_i was taken as the height of the vertical heat flux minimum. Finally, for particles that traveled outside the lateral boundaries of the computational domain, the velocities were found using the periodicity of the computed flow field.

b. Results and discussion

The computed CWIC fields for a surface source are compared with the predictions of surface-layer similarity (SLS) theory, and the results for a near-surface source ($z_{os}/z_i = 0.07$) are compared with the Willis and Deardorff (1976) convection tank data. The latter are ensemble-average values and have been shown to be a good fit to the mean of surface concentrations from two field experiments (Briggs 1988, 1993). The focus on surface and near-surface sources is intended as a stringent test of the LES–LSM approach since the surface region is where the SFS TKE fraction is large and where we might expect the most difficulty in matching theory and experimental data.

Figure 3 shows vertical profiles of the dimensionless CWIC, $C^y Uz_i/Q$, as a function of the dimensionless downwind distance

$$X = \frac{w_* x}{Uz_i} \tag{26}$$

for a near-surface source ($z_{os}/z_i = 0.07$). The model result for this source (solid line) gives a good overall fit to the data showing the dimensionless C^y to have a maximum value near the surface for $X \lesssim 0.5$; to attain an elevated maximum in C^y at $X \simeq 1.5$; and to approximate a vertically well-mixed distribution, $C^y Uz_i/Q \simeq 1$, by $X \sim 3$. The elevated maximum is a unique property of a highly convective PBL and is caused by the vertical inhomogeneity in σ_w combined with the large $T_L \sim z_i/w_*$, which generates a positive mean drift velocity

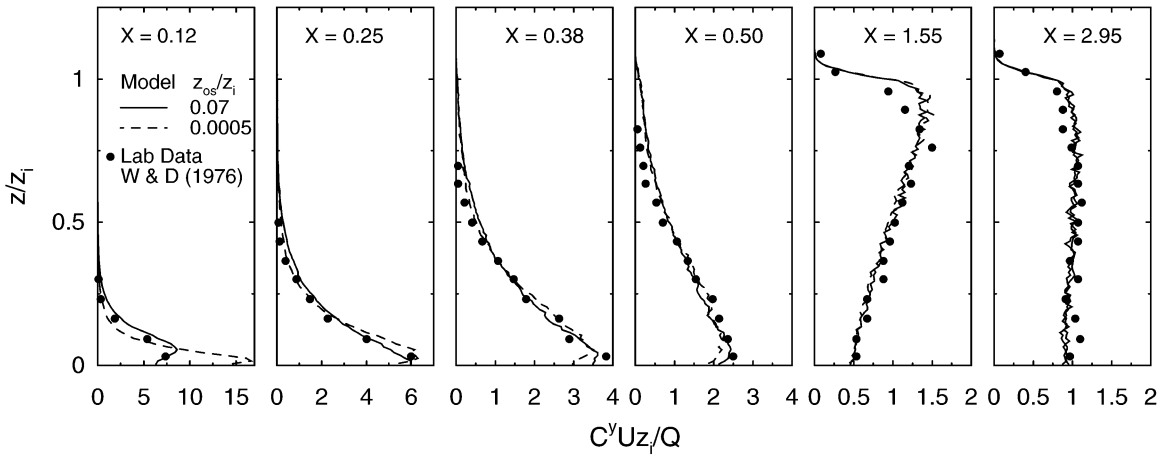

FIG. 3. Dimensionless CWIC as a function of dimensionless height at six downstream distances as denoted by the dimensionless distance X. Lagrangian model results for two source heights compared with Willis and Deardorff (1976; W&D) convection tank data where $z_{os}/z_i = 0.07$; model results for $C_0 = 3$.

(Sawford and Guest 1987; Weil 1990). The computed profiles were made for $C_0 = 3$, which was a best-fit value given by Du (1997) based on evaluation of LSMs with measurements from several different flows.

The modeled C^y profiles for a surface release (dashed line, Fig. 3) exhibit only small differences from those of the near-surface source except very close to the source ($X = 0.12$). Once dispersion occurs throughout a significant depth of the CBL, the effects of source height differences within the surface layer have small effects on the vertical distribution of C^y (see profiles for $X \geq 0.25$ or 0.38).

The dimensionless CWIC at the surface versus X is shown (Fig. 4) for three ways of modeling the SFS velocity: (a) no SFS velocity or $f_s = 0$, (b) the proposed model [Eqs. (15) and (22)] in section 3, and (c) a model [Eq. (15)] with $f_s = 1$, that is, no correction for the SFS TKE fraction. In (c), the assumed $f_s = 1$ means that the SFS time scale $T_{Ls} = 2\sigma_s^2/(C_0\epsilon) = \sigma_s^2 T_L/(\sigma_{av}^2 + \sigma_s^2)$, and thus T_{Ls} can be much smaller than T_L or T_{Lr}, especially at mid-CBL levels. The third approach was adopted by Weil et al. (2000) who found that a $C_0 = 1$ worked best in matching the Willis and Deardorff (1976, 1978) data. This approach also is akin to that used by Lamb (1978, 1982) who assumed $T_{Ls} = \Delta'/e_s^{1/2}$, where $\Delta' = (2/3)^{2/3}\Delta$; Lamb's $T_{Ls}(=0.76\Delta/e_s^{1/2})$ is about 50% of the value in Weil et al. (2000).

The surface CWIC results for the proposed model (Fig. 4b) agree well with the Willis and Deardorff (1976) data and show 1) a local surface CWIC maximum as expected for an elevated source, 2) an approach to the well-mixed CWIC ($C^y U z_i/Q = 1$) at $X \simeq 4$, and 3) an undershoot of the well-mixed value over the range $1 \leq X \leq 2$. The proposed model behavior is slightly better than that of the earlier model (Fig. 4c); the difference between them being primarily in the magnitude of the peak concentration. For both models (Figs. 4b and 4c), the CWIC profile exhibits little variation with C_0. This may be due to the SFS TKE being only a small fraction (20%) of the total TKE at this release height, although the fraction increases toward the surface (Fig. 2).

By comparison with the above results, the model without any SFS component (Fig. 4a) performs poorly. We note that the initial SFS velocities for the calculations in Figs. 4b,c are assumed to have a Gaussian PDF with zero mean. In the vertical direction, the negative SFS velocities are important in producing initial downwardly directed particle trajectories. Without such velocities, there is evidently an insufficient number of such trajectories since the maximum C^y at the surface (Fig. 4a) is only about one-half the value found in the experiments. In addition, the failure of this model (Fig. 4a) to achieve the well-mixed CWIC by $X \simeq 4$ demonstrates the importance of the surface SFS velocities in transporting particles to sufficient heights where the resolved velocities are larger and can dominate the motion. The small resolved velocities near the surface combined with the zero SFS velocities result in particles spending too much time near the surface and in higher-than-expected surface CWICs far downstream.

As another test of the Lagrangian model, we compare results for the CWIC downwind of a surface source with predictions of SLS theory (van Ulden 1978; Horst 1979; Horst and Weil 1992), which has been shown to agree well with field data. The theory is based on the M–O similarity profiles of mean wind, turbulence, and eddy diffusivity in the atmospheric surface layer. The CWIC field is given by $C^y(x, z) = AQ/[\overline{U}(x)\overline{z}_p] \exp(-z/b\overline{z}_p)^r$, where $\overline{U}(x)$ is the average wind speed over the plume, and A and b are functions of the shape parameter r, which generally lies in the range $1 \leq r \leq 2$. For strong convection, $r = A = b = 1$. The key variable in the theory is the mean plume height $\overline{z}_p(x)$, which is found from the scalar eddy diffusivity and mean wind profiles; details are given in Horst and Weil (1992). Since the similarity forms of the eddy diffusivity and wind profiles

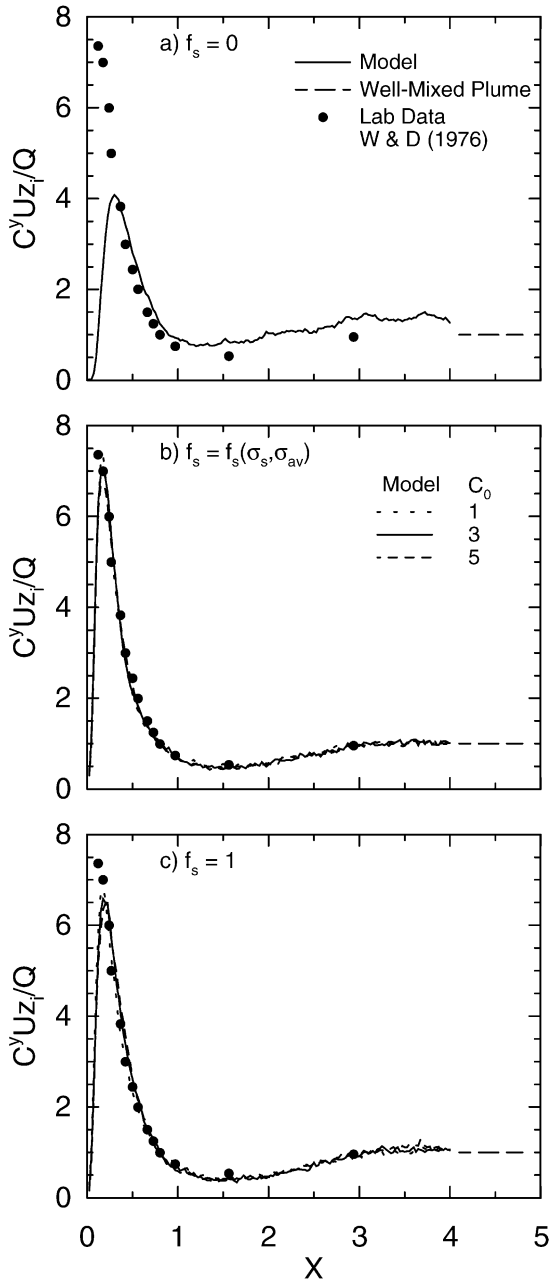

FIG. 4. Dimensionless CWIC at the surface as a function of dimensionless distance for a near-surface source ($z_{os}/z_i = 0.07$) in the CBL. (a)–(c) Lagrangian model results given for three ways of treating the random forcing in the SFS LSM and compared with Willis and Deardorff (1976) convection tank data. Key for well-mixed plume and data in (a) applies to (b) and (c); in (b) $f_s(\sigma_s, \sigma_{av}) = \langle\sigma_s^2\rangle/(\langle\sigma_{av}^2\rangle + \langle\sigma_s^2\rangle)$.

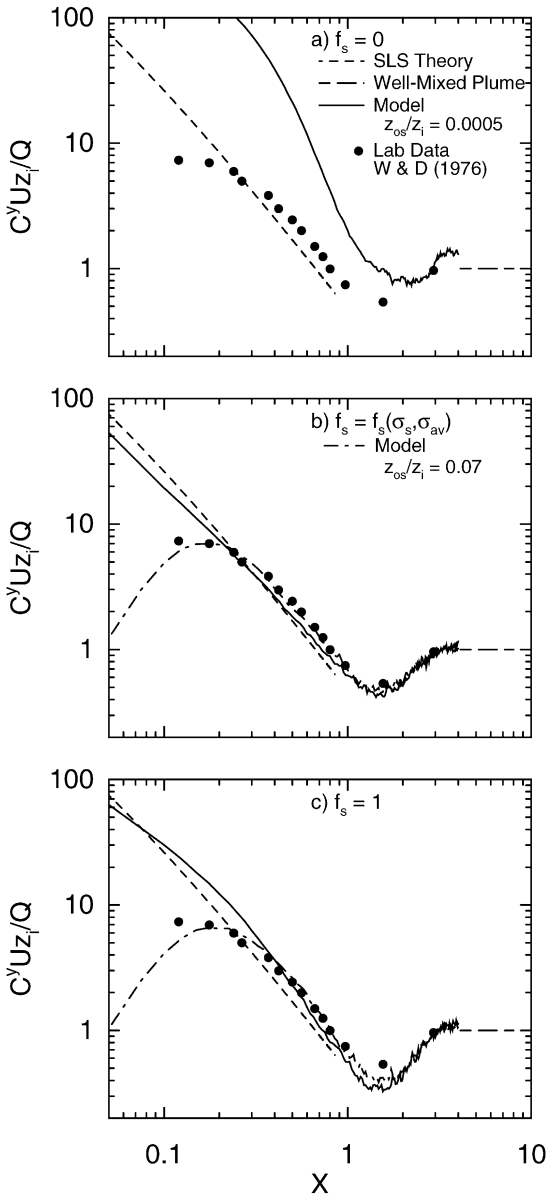

FIG. 5. Dimensionless CWIC at the surface as a function of dimensionless distance for a surface source in the CBL. (a)–(c) Three ways of treating the random forcing in the SFS LSM, same as in Fig. 4 with $C_0 = 3$ in (b) and (c); key in (a) applies to (b) and (c).

are assumed to apply, SLS theory ignores the different turbulence characteristics that exist in the CBL mixed layer and the effects of the capping inversion. Thus, the theory must be limited to short downwind distances, say, $X < 1$, before the presence of the inversion is felt.

Figure 5 presents the dimensionless CWIC at the surface as a function of X for a surface source and the same three SFS models used in Fig. 4. We judge the adequacy of the Lagrangian model based on comparisons of the modeled CWIC with SLS theory and laboratory data for a surface-layer source, $z_{os}/z_i = 0.07$. Use of the laboratory data is justified since 1) the data show the same variation with X as SLS theory over the range $0.2 \leq X \leq 1$ (Fig. 5), and 2) the modeled vertical profiles for $z_{os}/z_i = 0.0005$, 0.07 (solid, dashed lines, Fig. 2) agree approximately for $X \geq 0.25$ or 0.38.

In Fig. 5a, one can see that the model with no SFS velocity substantially overpredicts SLS theory and the

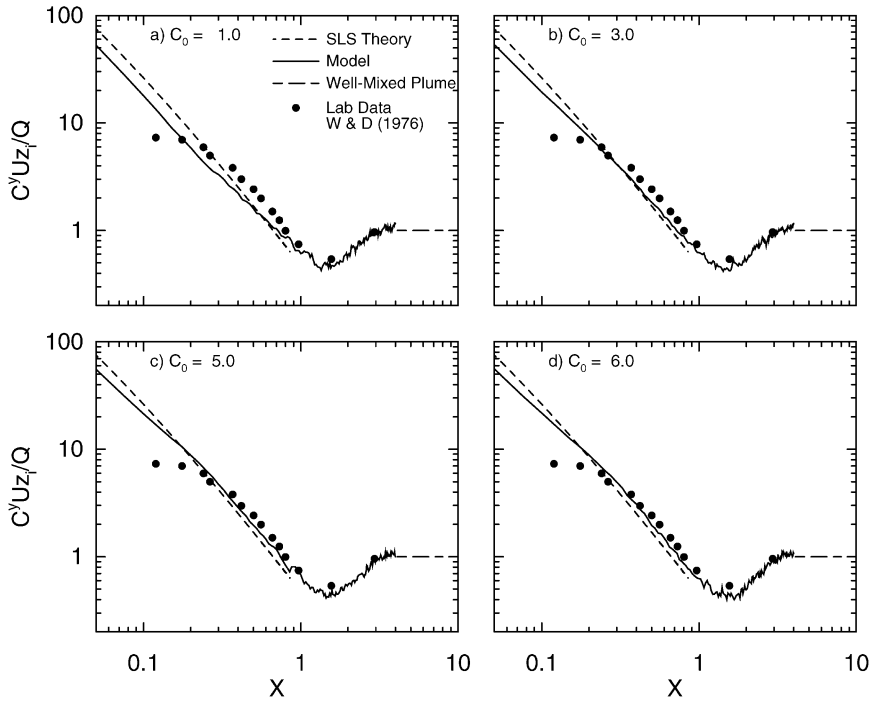

FIG. 6. Surface values of dimensionless CWIC vs dimensionless distance for a surface source in the CBL with C_0 as a parameter. Results for proposed model of SFS random forcing with $f_s = \langle\sigma_s^2\rangle/(\langle\sigma_{sv}^2\rangle + \langle\sigma_s^2\rangle)$.

laboratory data, and it also overestimates the CWIC at $X = 4$ as found for the elevated source (Fig. 4a). This demonstrates again the need for including the SFS velocities in modeling dispersion from surface and near-surface sources. In Fig. 5, one also can see that the proposed model (Fig. 5b, solid line) agrees well with SLS theory and the data for $0.2 < X \lesssim 3$ and better than predictions from the earlier model with $f_s = 1$ (Fig. 5c). For the proposed model, we believe that the underestimation of the SLS curve near the source ($X < 0.2$, Fig. 5b) is due to the assumed isotropic stress tensor in the SFS model. For a near-surface source, the short-range dispersion is dominated by the SFS model since the initial resolved velocities are small. Recent field observations (Sullivan et al. 2003) show that the SFS variances are anisotropic and match measurements from the neutral surface layer with $\sigma_{su}^2/\sigma_{is}^2 \simeq 1.5$, $\sigma_{sv}^2/\sigma_{is}^2 \simeq 1$, and $\sigma_{sw}^2/\sigma_{is}^2 \simeq 0.5$, where σ_{is}^2 is the variance for isotropic turbulence. We speculate that a halving of the SFS vertical velocity variance in the Lagrangian model would increase the near-source CWIC by about 40% (Fig. 5b), thus providing better agreement with SLS theory at short range. (The modifications necessary for including an anisotropic SFS model are postponed for future work.)

The proposed model exhibits a weak variation in the surface CWIC with C_0 (Fig. 6), which we view as a positive attribute. The primary range of C_0 found in other studies is $2 \leq C_0 \leq 6$ (Du 1997; Sawford 1991; Thomson 1987; Wilson and Sawford 1996) with a typical or best-fit value of $\simeq 3$. Here, the results for $C_0 = 1$ have been included because that was the best-fit value found for the earlier model (Fig. 7). For the proposed model, the results for $C_0 = 1$ (Fig. 6a) are perhaps the most different from the others. In contrast, the earlier model (Fig. 7) exhibits progressively poorer agreement with SLS theory and laboratory data as C_0 increases from 1 to 6. The poorer agreement with the larger C_0s (2–6) differs from the findings reported by Du (1997) and others.

We have tested the Lagrangian dispersion model and LSM directly using mean concentration fields from SLS theory and laboratory experiments. An alternative approach for evaluating the LSM would be to conduct a fine-mesh LES at 1- or 2-m resolution and then to filter the results to generate new ''resolved'' and ''subfiltered'' velocities for a coarse mesh. This would allow one to use the known particle velocity and position time histories from the fine mesh to test the LSM performance on the coarse mesh; the use of fine- and coarse-mesh results in this way is commonly referred to as a priori testing (e.g., Piomelli et al. 1990). This alternative approach, which could provide valuable insight into the LSM behavior, is reserved for future work.

5. Summary and conclusions

A Lagrangian dispersion model driven by LES velocity fields was presented for passive particle dispersion in the PBL. In this combined LES–Lagrangian sto-

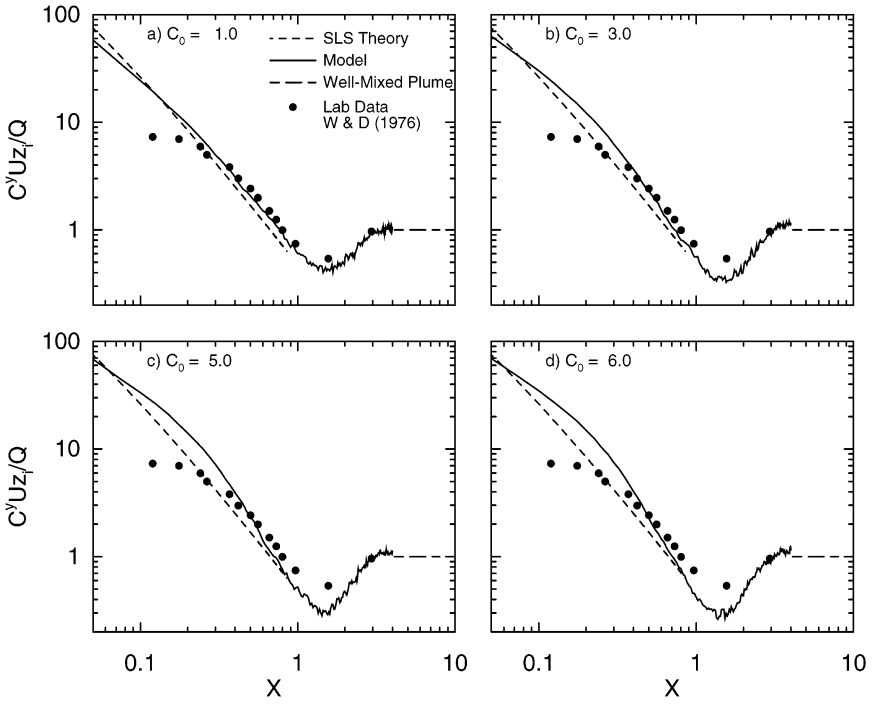

FIG. 7. Surface values of dimensionless CWIC vs dimensionless distance for a surface source in the CBL with C_0 as a parameter. Results from SFS random forcing model with $f_s = 1$.

chastic model (LSM), the total velocity was divided into resolved (filtered) and unresolved (subfilter scale, SFS) velocities. The random SFS velocity was based on an adaptation of Thomson's (1987) LSM in which the ensemble-mean velocity and velocity variances were replaced by the resolved velocity and SFS variances, respectively. The random SFS velocity forcing has an amplitude determined by the SFS fraction of the total turbulent kinetic energy (TKE); in principle, the fraction can range from 0 for fully resolved turbulence to 1 for completely parameterized turbulence and is ~0.15 in the bulk of the CBL simulated here.

For the proposed model, the crosswind-integrated concentration (CWIC) fields were in good agreement with 1) surface-layer similarity (SLS) theory for a surface source in the CBL and 2) convection tank measurements of the CWIC for an elevated release ($z_{os}/z_i = 0.07$) in the CBL surface layer. The second comparison included the modeled evolution of the vertical profile shape with downstream distance, which showed the attainment of an elevated CWIC maximum and a vertically well-mixed CWIC far downstream, in agreement with the tank data. For the proposed model, the variation of the surface CWIC with distance agreed with the tank data and SLS theory better than an earlier model in which the SFS fraction of the TKE was assumed to be 1, and significantly better than a model that ignored the SFS velocities altogether. The results for the proposed model were achieved with a Lagrangian structure function constant ($C_0 = 3$) in agreement with that found in earlier studies of LSMs, and the results were rather insensitive to C_0 over the range $2 \leq C_0 \leq 6$.

Acknowledgments. We thank S.-W. Kim, M. W. Rotach, and B. L. Sawford for helpful comments on the Lagrangian model and anonymous reviewers for useful comments on the paper. The use of finer-scale resolution LES to evaluate the LSM (discussed at end of section 4b) was suggested by one of the reviewers. J. C. Weil is grateful for support from the U.S. Army Research Office under Grant DAAG55-97-1-0259.

REFERENCES

Briggs, G. A., 1988: Analysis of diffusion field experiments. *Lectures on Air Pollution Modeling,* A. Venkatram and J. C. Wyngaard, Eds., Amer. Meteor. Soc., 63–117.

——, 1993: Plume dispersion in the convective boundary layer. Part II: Analyses of CONDORS field experiment data. *J. Appl. Meteor.,* **32,** 1388–1425.

Deardorff, J. W., 1972: Numerical investigation of neutral and unstable planetary boundary layers. *J. Atmos. Sci.,* **29,** 91–115.

——, 1974: Three-dimensional numerical study of the height and mean structure of a heated planetary boundary layer. *Bound.-Layer Meteor.,* **7,** 81–106.

——, 1980: Stratocumulus-capped mixed layers derived from a three-dimensional model. *Bound.-Layer Meteor.,* **18,** 495–527.

——, and G. E. Willis, 1985: Further results from a laboratory model of the convective planetary boundary layer. *Bound.-Layer Meteor.,* **32,** 205–236.

Du, S., 1997: Universality of the Lagrangian velocity structure function constant (C_0) across different kinds of turbulence. *Bound.-Layer Meteor.,* **83,** 207–219.

Durbin, P. A., 1983: Stochastic differential equations and turbulent dispersion. NASA Reference Publication 1103, 69 pp.

Gardiner, C. W., 1990: *Handbook of Stochastic Methods for Physics, Chemistry and the Natural Sciences*. Springer-Verlag, 442 pp.

Gopalakrishnan, S. G., and R. Avissar, 2000: An LES study of the impacts of land surface heterogeneity on dispersion in the convective boundary layer. *J. Atmos. Sci.,* **57,** 352–371.

Horst, T. W., 1979: Lagrangian similarity modeling of vertical diffusion from a ground-level source. *J. Appl. Meteor.,* **18,** 733–740.

——, and J. C. Weil, 1992: Footprint estimation for scalar flux measurements in the atmospheric surface layer. *Bound.-Layer Meteor.,* **59,** 279–296.

Lamb, R. G., 1978: A numerical simulation of dispersion from an elevated point source in the convective planetary boundary layer. *Atmos. Environ.,* **12,** 1297–1304.

——, 1982: Diffusion in the convective boundary layer. *Atmospheric Turbulence and Air Pollution Modeling,* F. T. M. Nieuwstadt and H. van Dop, Eds., Reidel, 159–229.

Mason, P. J., 1992: Large-eddy simulation of dispersion in convective boundary layers with wind shear. *Atmos. Environ.,* **26A,** 1561–1571.

——, 1994: Large-eddy simulation: A critical review of the technique. *Quart. J. Roy. Meteor. Soc.,* **120,** 1–26.

Moeng, C.-H., and J. C. Wyngaard, 1988: Spectral analysis of large-eddy simulations of the convective boundary layer. *J. Atmos. Sci.,* **45,** 3573–3587.

——, and P. P. Sullivan, 1994: A comparison of shear- and buoyancy-driven planetary boundary layers. *J. Atmos. Sci.,* **51,** 999–1022.

Monin, A. S., and A. M. Yaglom, 1975: *Statistical Fluid Mechanics: Mechanics of Turbulence*. Vol. 2, MIT Press, 874 pp.

Pasquill, F. A., and F. B. Smith, 1983: *Atmospheric Diffusion*. 3d ed. Wiley, 437 pp.

Piomelli, U., T. A. Zang, C. G. Speziale, and M. Y. Hussaini, 1990: On the large-eddy simulation of transitional wall-bounded flows. *Phys. Fluids,* **A2,** 257–265.

Rodean, H. C., 1996: *Stochastic Lagrangian Models of Turbulent Diffusion. Meteor. Monogr.,* No. 48, Amer. Meteor. Soc., 84 pp.

Sawford, B. L., 1991: Reynolds number effects in Lagrangian stochastic models of turbulent diffusion. *Phys. Fluids,* **A3,** 1577–1586.

——, and F. M. Guest, 1987: Lagrangian stochastic analysis of flux-gradient relationships in the convective boundary layer. *J. Atmos. Sci.,* **44,** 1152–1165.

Sullivan, P. P., T. W. Horst, D. H. Lenschow, C.-H. Moeng, and J. C. Weil, 2003: Structure of subfilter-scale fluxes in the atmospheric surface layer with application to large-eddy simulation modeling. *J. Fluid Mech.,* **482,** 101–139.

Taylor, G. I., 1921: Diffusion by continuous movements. *Proc. London Math. Soc.,* **20,** 196–212.

Tennekes, H., and J. L. Lumley, 1972: *A First Course in Turbulence*. MIT Press, 300 pp.

Thomson, D. J., 1987: Criteria for the selection of stochastic models of particle trajectories in turbulent flows. *J. Fluid Mech.,* **180,** 529–556.

van Ulden, A. A. P., 1978: Simple estimates for vertical dispersion from sources near the ground. *Atmos. Environ.,* **12,** 2125–2129.

Weil, J. C., 1990: A diagnosis of the asymmetry in top-down and bottom-up diffusion using a Lagrangian stochastic model. *J. Atmos. Sci.,* **47,** 501–515.

——, P. P. Sullivan, and C.-H. Moeng, 2000: Lagrangian modeling of dispersion in the convective boundary layer over a range of stability. Preprints, *11th Joint Conf. on the Applications of Air Pollution Meteorology with the A&WMA,* Long Beach, CA, Amer. Meteor. Soc., 30–34.

Willis, G. E., and J. W. Deardorff, 1976: A laboratory model of diffusion into the convective planetary boundary layer. *Quart. J. Roy. Meteor. Soc.,* **102,** 427–445.

——, and ——, 1978: A laboratory study of dispersion from an elevated source within a modeled convective planetary boundary layer. *Atmos. Environ.,* **12,** 1305–1312.

Wilson, J. D., and B. L. Sawford, 1996: Review of Lagrangian stochastic models for trajectories in the turbulent atmosphere. *Bound.-Layer Meteor.,* **78,** 191–220.